Interactions among DIV voltage-sensor movement, fast inactivation, and resurgent Na current induced by the $Na_V\beta4$ open-channel blocking peptide

Amanda H. Lewis[1,2] and Indira M. Raman[1,2]

[1]Interdepartmental Biological Sciences Program and [2]Department of Neurobiology, Northwestern University, Evanston, IL 60208

Resurgent Na current flows as voltage-gated Na channels recover through open states from block by an endogenous open-channel blocking protein, such as the $Na_V\beta4$ subunit. The open-channel blocker and fast-inactivation gate apparently compete directly, as slowing the onset of fast inactivation increases resurgent currents by favoring binding of the blocker. Here, we tested whether open-channel block is also sensitive to deployment of the DIV voltage sensor, which facilitates fast inactivation. We expressed $Na_V1.4$ channels in HEK293t cells and assessed block by a free peptide replicating the cytoplasmic tail of $Na_V\beta4$ (the "β4 peptide"). Macroscopic fast inactivation was disrupted by mutations of DIS6 (L443C/A444W; "CW" channels), which reduce fast-inactivation gate binding, and/or by the site-3 toxin ATX-II, which interferes with DIV movement. In wild-type channels, the β4 peptide competed poorly with fast inactivation, but block was enhanced by ATX. With the CW mutation, large peptide-induced resurgent currents were present even without ATX, consistent with increased open-channel block upon depolarization and slower deactivation after blocker unbinding upon repolarization. The addition of ATX greatly increased transient current amplitudes and further enlarged resurgent currents, suggesting that pore access by the blocker is actually decreased by full deployment of the DIV voltage sensor. ATX accelerated recovery from block at hyperpolarized potentials, however, suggesting that the peptide unbinds more readily when DIV voltage-sensor deployment is disrupted. These results are consistent with two open states in Na channels, dependent on the DIV voltage-sensor position, which differ in affinity for the blocking protein.

The Journal of General Physiology

INTRODUCTION

Voltage-gated Na channels open in response to depolarization, generating transient Na currents, which produce the upstroke of the action potential. In most excitable cells, open Na channels rapidly become nonconducting, usually by making transitions to fast-inactivated states. In some neurons, however, open channels are instead blocked by a proteinaceous blocking particle that terminates current flow and prevents fast inactivation. In these neurons, repolarization reopens Na channels, as permeating Na ions expel the blocking protein and elicit "resurgent" current that is the electrical signature of block and unblock. Displacement of the blocking protein restores channel availability and facilitates repetitive action potential firing (Raman and Bean, 1997, 2001; Khaliq et al., 2003; Aman and Raman, 2010). Block is contingent on channel opening, and both fast inactivation and deactivation (closure) are contingent on channels not being blocked (Raman and Bean, 2001).

The pore, voltage sensor, and fast-inactivation gate are contained within the Na channel α subunit, whereas the open-channel blocker is a separate but associated protein, identified in some neurons as the $Na_V\beta4$ subunit (Yu et al., 2003; Grieco et al., 2005; Bant and Raman, 2010). Nevertheless, expression of a blocking protein is not always sufficient to generate resurgent current. For instance, in Purkinje neurons, loss of the $Na_V1.6$ α subunit nearly abolishes resurgent current, even when the blocker and other α subunits remain present (Raman et al., 1997). Likewise, in dorsal root ganglion neurons, which also have an endogenous blocker, expression of $Na_V1.4$ fails to induce resurgent current through those channels (Cummins et al., 2005; Jarecki et al., 2010). Slowing macroscopic inactivation with site-3 toxins, however, augments resurgent current in WT neurons and permits it to flow through other subunits in $Na_V1.6$-null Purkinje cells (Grieco and Raman, 2004; Klinger et al., 2012; Liu et al., 2012; Sittl et al., 2012). Similarly, in channels expressing pain syndrome–linked mutations that slow the onset of fast inactivation, blocker-induced resurgent current amplitudes are increased (Jarecki et al., 2010; Theile et al., 2011). These observations raise the question of what mechanisms underlie the mutual antagonism of fast inactivation and open-channel block.

Correspondence to Indira M. Raman: i-raman@northwestern.edu

The Rockefeller University Press $30.00
J. Gen. Physiol. Vol. 142 No. 3 191–206
www.jgp.org/cgi/doi/10.1085/jgp.201310984

A simple idea is that binding of the fast-inactivation gate occludes the binding site of the open-channel blocker and vice versa. Structurally, however, inactivation is a multistep process. Voltage-gated Na channels have four homologous domains (DI–DIV); in each, the fourth transmembrane segment (S4) serves as part of a larger voltage-sensing domain (S1–S4) (Stühmer et al., 1989). Channel opening requires outward movement ("deployment") of the voltage sensors of DI, DII, and DIII (Chanda and Bezanilla, 2002), and possibly partial deployment of DIV (Horn et al., 2000; Campos et al., 2008). Presumably, these channel-opening movements are necessary for the open-channel blocker to bind. Deployment of the DIV voltage sensor (henceforth "DIVS4"), however, also favors fast inactivation, mediated by the intracellular DIII–DIV linker (Chahine et al., 1994; Eaholtz et al., 1994; Sheets et al., 1999). Recent evidence also indicates that partial or full deployment of DIVS4 converts channels from high conductance to lower conductance open states (Goldschen-Ohm et al., 2013). Interestingly, site-3 toxins, which slow inactivation and augment resurgent current, act in part by restricting DIVS4 movement (el-Sherif et al., 1992; Rogers et al., 1996; Sheets et al., 1999), raising the possibility that open-channel block may be sensitive to DIVS4 movement as well as to binding of the fast-inactivation gate per se.

To compare the sensitivity of open-channel block to DIVS4 position and fast-inactivation gate binding, we made two separate manipulations to reduce fast inactivation of $Na_V1.4$ channels in HEK cells, namely, mutating a putative docking site of the inactivation gate and applying the site-3 toxin ATX-II. Even with fast inactivation disrupted, open-channel block by the β4 peptide is further influenced by DIVS4. We find that restricting DIVS4 movement increases the peptide's accessibility to the pore, but the affinity of the blocker is greater with deployment unimpeded.

MATERIALS AND METHODS

Channel constructs and expression

All experiments were performed on WT human $Na_V1.4$ (provided by S. Cannon, University of Texas-Southwestern, Dallas, TX) expressed in HEK293t cells. The inactivation-deficient mutant L443C/A444W ("CW"; Wang et al., 2003) was constructed with the QuikChange XL Site-Directed Mutagenesis kit (Agilent Technologies) and verified by sequencing at the Northwestern University Genomics Core facility. HEK293t cells (Thermo Fisher Scientific) were grown to 50% confluence in Dulbecco's modified Eagle's medium (with 10% FBS and MEM nonessential amino acids) and transfected 2 d before recording using the CalPhos Mammalian Transfection kit (Takara Bio Inc.). $Na_V1.4$ was cotransfected with $Na_V\beta1$ to increase current density and GFP as a marker of transfected cells in a 1:2:0.2 molar ratio. 24–30 h after transfection, cells were replated at low density onto poly-L-lysine–coated coverslips for recording the next day.

Recording and analysis

Parafilm-wrapped borosilicate pipettes (1.5–2.5 MΩ) were filled with filtered intracellular solution that contained (mM): 108 $CsCH_3SO_3$, 9 NaCl, 4.5 TEA-Cl, 1.8 $MgCl_2$, 0.45 EGTA, 9 HEPES, 23 sucrose, 14 Tris-creatine PO_4, 4 MgATP, and 0.3 Tris-GTP, pH 7.35 with CsOH. Where indicated, 200 µM of the extended mouse β4 peptide (KKLITFILKKTREKKKECLV; Thermo Fisher Scientific) was added to the intracellular solution and allowed to diffuse into the cell until responses were stable (typically 5 min). Whole cell voltage-clamp recordings were made at room temperature with an amplifier (Multiclamp 700B; Molecular Devices) and pClamp 9.2, sampled at 50 kHz, and filtered at 6 kHz. Series resistance was compensated at >65%.

Extracellular solutions were controlled with a series of gravity-driven flow pipes. The control extracellular solution contained (mM): 50 NaCl, 2 $CaCl_2$, 2 $MgCl_2$, 10 HEPES, 100 TEA-Cl, and 5 glucose, pH 7.35 with TEA-OH. This reduced Na concentration improved fidelity of voltage clamp, especially in inactivation-deficient cells, and increased the stability of peptide block (Afshari et al., 2004; Aman and Raman, 2010). To delay the onset of fast inactivation, 500 nM of the site-3 toxin ATX-II (ATX; Alomone Labs) was added to the extracellular solution as indicated and applied until responses were stable (typically 1 min) before recording. For reverse gradient experiments, intracellular Cs was replaced by Na (mM: 108 $NaCH_3SO_3$, 9 NaCl, 4.5 TEA-Cl, 9 HEPES, 1.8 $MgCl_2$, 30 sucrose, 14 Tris-creatine PO_4, 4 MgATP, and 0.3 Tris-GTP, pH 7.33 with NaOH; total Na = 115), and extracellular Na was replaced by TEA (mM: 15 NaCl, 135 TEA-Cl, 2 $MgCl_2$, 2 $CaCl_2$, 10 HEPES, and 10 glucose, pH 7.32 with CsOH). In all recordings, TTX-sensitive Na current was isolated by subtracting currents recorded in 900 nM TTX (Alomone Labs). Unless indicated, all chemicals were from Sigma-Aldrich.

Data were analyzed with Igor Pro 6.0 (WaveMetrics) and reported as mean ± SEM. Statistical significance was assessed by Student's two-tailed t tests, and significance was taken as $P < 0.05$. All comparisons ±ATX are paired; others are unpaired. To control for variance in current density, currents were normalized as indicated to the transient current evoked at 0 mV. If conductance was not maximal at 0 mV, the current at 0 mV was corrected by dividing by the fractional conductance at 0 mV, and this value is also reported. To assess activation properties, conductance–voltage plots were normalized to the maximal conductance and fit with a Boltzmann function, $G/G_{max} = 1/(1 + \exp(-(V - V_{1/2})/k))$, where G is conductance, G_{max} is the maximal conductance, $V_{1/2}$ is the half-maximal voltage of activation, and k is the slope factor. Steady-state inactivation curves were normalized to peak current and fit with a modified Boltzmann of the form $I = F_{ss} + (1 - F_{ss})/(1 + \exp((V - V_{1/2})/k))$, where I is the normalized current at 0 mV, $V_{1/2}$ is the half-maximal voltage of inactivation, k is the slope factor, and F_{ss} is the fraction of noninactivating current. Unsubtracted capacitive artifacts and some tail currents in recovery experiments have been digitally blanked for clarity.

For recovery experiments, channels were conditioned at either 0 mV for 25 ms or +60 mV for 10 ms, and then repolarized to −110 mV for varying intervals. To estimate the fractional recovery of channels that had become nonconducting, currents were first normalized to the response to the conditioning pulse for each trace. The fraction of current that did not inactivate during the conditioning step (F_{ss}) was either measured at the end of the step (for conditioning at 0 mV) or calculated from the tail current elicited by repolarization to 0 mV (for conditioning at +60 mV). The tail currents were corrected for the fractional conductance evoked by a direct depolarization to 0 mV because at +60 mV, conductance is maximal in all conditions (both channel types, ±ATX, ±β4 peptide), but direct depolarization to 0 mV evokes a submaximal conductance in some conditions. The F_{ss} value was then subtracted from both the peak response to the

conditioning step (=1 − F_{ss}) and peak response to the test step to 0 mV (=F_{test} − F_{ss}). Recovery was calculated as the ratio of these values, i.e., (F_{test} − F_{ss})/(1 − F_{ss}), and the recovery profile was fit with the equation $I = y_0 - (A_{fast}*\exp(-x/\tau_{fast}) + (1 - A_{fast})*\exp(-x/\tau_{slow}))$, where A_{fast} and τ_{fast} are the amplitude and time constant of the briefer phase of recovery, (1 − A_{fast}) and τ_{slow} are the amplitude and time constant of the slower phase of recovery, and y_0 is the offset (usually 1, barring a delay in recovery). Data are reported as the fractional recovery of nonconducting channels.

RESULTS

To test how the fast-inactivation gate and DIVS4 movement each influence the blockade of open Na channels by the β4 peptide, we recorded from WT, inactivation-deficient, and toxin-modified $Na_V1.4$ channels coexpressed with $Na_V\beta1$ in HEK293t cells. We began by assessing macroscopic inactivation and its modulation by ATX in WT channels, without the addition of a blocker. Whole-cell, voltage-clamped currents decayed rapidly and profoundly upon depolarization (Fig. 1, A and B). To facilitate comparison across conditions, some of which showed biphasic time courses of inactivation, we characterized the early and late phases of decay by two measures: the time for the peak current to decay by 25% ("25% decay time") and the percentage of the peak current remaining at 100 ms of depolarization ("current at 100 ms"). For WT channels depolarized to 0 mV, the 25% decay time was 0.28 ± 0.02 ms, and recovery at 100 ms was only 0.31 ± 0.09% (n = 6; Fig. 1, C and D). Next, the same cells were exposed to ATX, which binds extracellularly and alters channel gating in part by impeding the movement of DIVS4 to its activated position (el-Sherif et al., 1992; Rogers et al., 1996; Sheets et al., 1999). 500 nM ATX slowed the initial component of decay at 0 mV, such that the 25% decay time was prolonged to 0.97 ± 0.08 ms ($P < 0.0001$; n = 6; paired; Fig. 1, A–C), and the current at 100 ms increased to 1.49 ± 0.34% ($P < 0.01$; Fig. 1 D). The peak currents also increased slightly (Fig. 1 A; quantified below). The ATX-induced changes in inactivation time, peak current, and steady-state current are consistent with those reported previously for skeletal muscle Na channels (Chahine et al., 1996).

Next, to destabilize fast inactivation without directly disrupting DIVS4 deployment, we substituted two residues at the C-terminal end of DIS6, L443C/A444W (Wang et al., 2003), which we refer to as "CW channels." These mutations largely prevent macroscopic inactivation, particularly of outward Na currents measured with reversed gradients. They are thought to alter the binding site for the fast-inactivation gate (Wang et al., 2003, 2004), although other aspects of the channels, like intersubunit coupling (Long et al., 2005), may also be affected. In control solutions, in which Na current is inward at voltages below +45 mV, Na currents of CW channels showed a clear, biphasic inactivation phase but decayed much more slowly than in WT channels. At 0 mV, the 25% decay time was prolonged by more than an order of magnitude to 3.90 ± 0.31 ms, and the current at 100 ms was 22.7 ± 2.2% (Fig. 1, A–D; n = 5). Multiple factors may contribute to the current decay that remains in CW channels, such as entry into slow-inactivated states, conversion of the channels from high conductance to low conductance states (Goldschen-Ohm et al., 2013), and/or weak but nonzero association of the intact fast-inactivation gate with its mutated

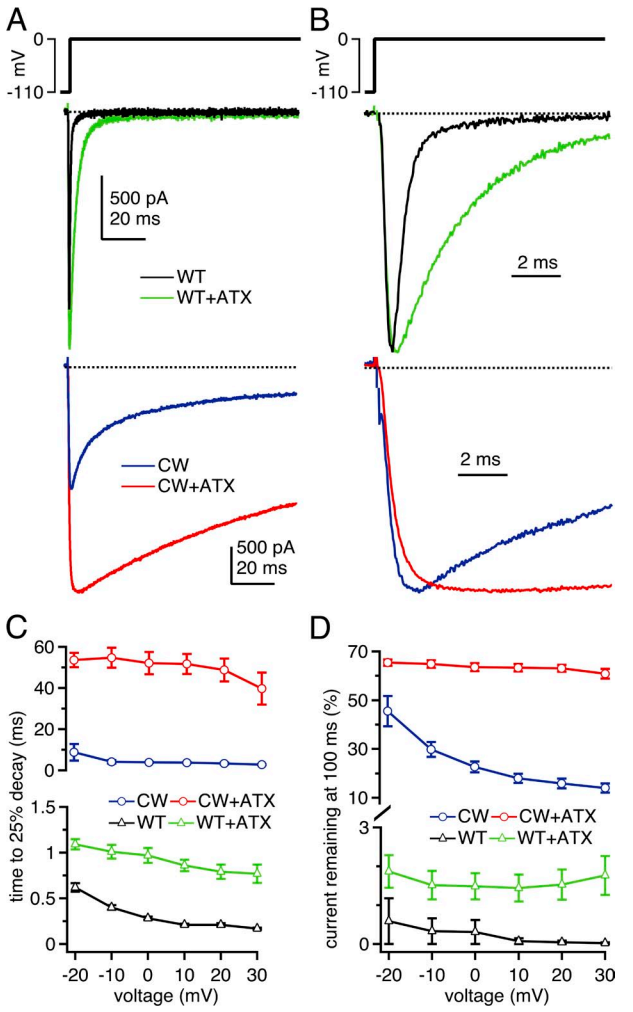

Figure 1. Macroscopic Na currents through WT, CW, and ATX-modified $Na_V1.4$ channels. (A; top) Voltage protocol. (Middle) Representative whole cell voltage-clamped Na currents through WT $Na_V1.4$ channels in control solutions (black) and with 500 nM ATX applied extracellularly (green). (Bottom) Representative Na currents through $Na_V1.4$ L443C/A444W (CW) channels in control solutions (blue) and with ATX (red). (B) Currents as in A, except normalized to peak. (C) Mean decay rate of Na currents as a function of voltage, measured as time for currents to decay by 25% of the peak current amplitude. Note different scales on upper and lower graphs. (D) Mean current remaining after 100 ms of depolarization, measured over last 1 ms of voltage step, relative to the peak transient current at that voltage. Within-cell comparisons ±ATX for each cell; WT, n = 6; CW, n = 5.

binding site. As in WT channels, ATX slowed the fast component of decay of CW channels (Fig. 1 A). In ATX, the 25% decay time at 0 mV was increased by another order of magnitude to 52.2 ± 5.4 ms, and the current at 100 ms nearly tripled to 63.5 ± 1.7% (n = 5; P < 0.001; both measures).

ATX also enlarged the peak currents in both channel types, although to different extents. In WT channels, peak currents at 0 mV increased by 25.3 ± 5.9% (Figs. 1 A and 2 A). This change can be partly attributed to a slight hyperpolarization of the voltage dependence of activation (P < 0.001; Table 1 and Fig. 2 C), which led a larger proportion of the total conductance, G_{max}, to be activated at 0 mV in ATX. Additionally, G_{max} itself increased by 16.9 ± 4.9% (P < 0.05). ATX also slightly negatively shifted and flattened the voltage dependence of inactivation (Table 2; $V_{1/2}$, P = 0.04; k, P < 0.001). Despite slowing inactivation, ATX did not measurably change the noninactivating fraction of current, as estimated from the Boltzmann fits (P = 0.17), suggesting

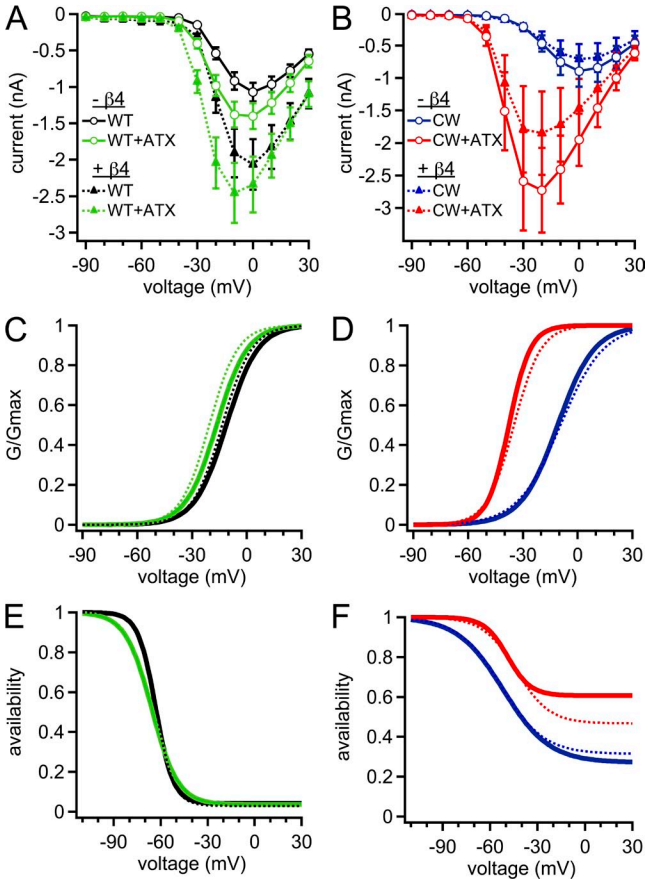

Figure 2. Activation and inactivation properties of WT, CW, and ATX-modified Na channels. (A) Mean current–voltage relation for WT (black) and ATX-modified WT (green) Na channels. In all panels, solid lines are without the β4 peptide, and dotted lines are with the β4 peptide. (B) Mean current–voltage relation for CW (blue) and ATX-modified (red) CW Na channels. (C) Peak conductance curve for WT and ATX-modified WT channels; Boltzmann function with mean $V_{1/2}$ and k parameters. (D) As in C, for CW and ATX-modified CW channels. (E) Steady-state inactivation curves for WT channels ±ATX; Boltzmann function with mean $V_{1/2}$, k, and steady-state parameters. (F) As in E, for CW channels ±ATX. Within-cell comparisons ±ATX for each cell; WT, n = 6; CW, n = 5.

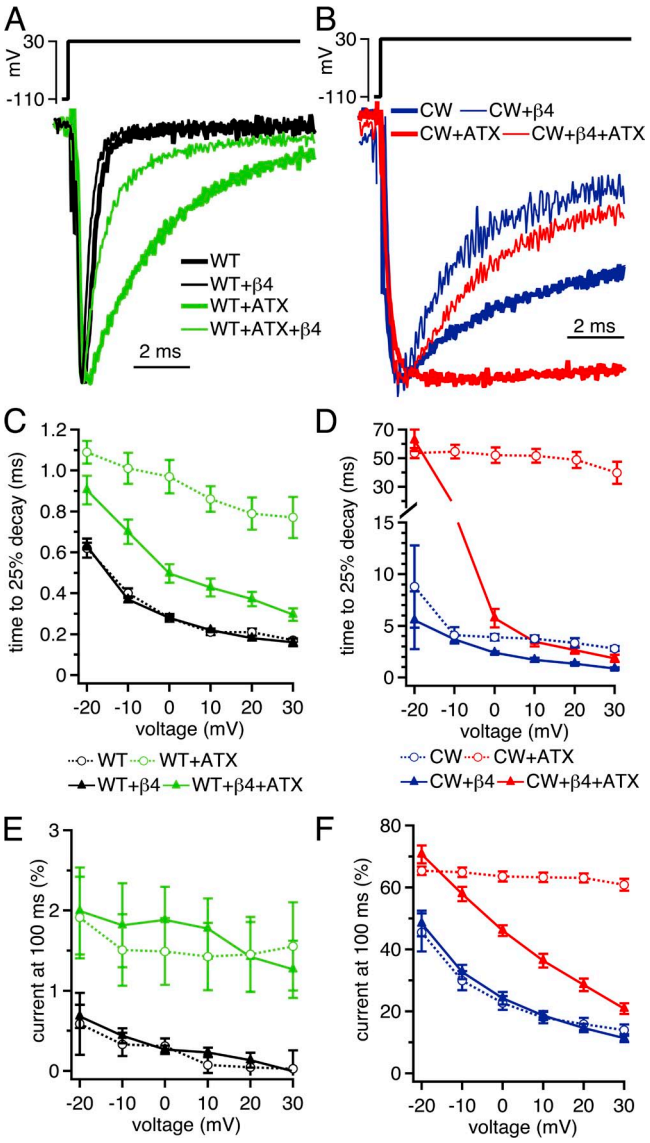

Figure 3. β4 peptide–mediated acceleration of current decay and reduction of steady-state current in CW channels. (A) Voltage protocol (top) and representative transient Na currents in WT (black) and ATX-modified WT (green), in the absence and presence of 200 µM β4 peptide. Currents normalized to peak current amplitude for comparison. (B) As in A, with CW (blue) and ATX-modified CW (red) channels. (C) Mean decay rate of WT Na currents as a function of voltage ±β4 peptide and ±ATX. Currents measured as time for currents to decay by 25% of the peak current amplitude. (D) As in C, for CW Na channels. (E) Mean current remaining after 100 ms of depolarization, measured over last 1 ms of voltage step, relative to the peak transient current at that voltage. (F) As in E, for CW channels. Within-cell comparisons ±ATX for each cell; WT, n = 6; CW, n = 5; WT plus β4, n = 5; CW plus β4, n = 6.

TABLE 1

Parameters of activation

Condition	−β4 Peptide			+β4 Peptide			P-value (−β4 vs. +β4)		
	$V_{1/2}$	k	G_{max}	$V_{1/2}$	k	G_{max}	$V_{1/2}$	k	G_{max}
	mV	*mV*	*nS*	*mV*	*mV*	*nS*			
WT − ATX (n = 6, 5)	−11.2 ± 0.7	8.7 ± 0.2	28.1 ± 3.3	−13.5 ± 0.5	8.1 ± 0.3	38.5 ± 10.9	<0.05	0.1	0.3
WT + ATX (n = 6, 5)	−16.5 ± 0.9	8.4 ± 0.1	33.0 ± 4.2	−20.5 ± 1.1	7.8 ± 0.5	40.1 ± 10.9	<0.05	0.2	0.5
CW − ATX (n = 5, 6)	−10.9 ± 0.8	10.0 ± 0.3	24.7 ± 7.3	−9.4 ± 1.0	11.7 ± 0.3	20.2 ± 6.4	0.3	<0.005	0.7
CW + ATX (n = 5, 6)	−35.6 ± 2.1	5.6 ± 0.5	45.7 ± 10.1	−34.9 ± 1.4	7.4 ± 0.5	31.2 ± 10.2	0.8	<0.05	0.5

that ATX slows but does not prevent DIVS4 movement in WT channels.

ATX had a much larger effect on current amplitudes in CW channels. Peak amplitudes at 0 mV increased greatly in ATX, to 236 ± 17% of control. As in WT channels, this increase could be partly attributed to a large hyperpolarizing shift in the $V_{1/2}$ of activation (Fig. 2, B and D, and Table 1). A substantial contribution, however, also came from the more than doubling of G_{max}, which rose to 211 ± 24% of control. ATX did not affect the voltage dependence of inactivation (P = 0.10; Fig. 2 F). Consistent with the measured current at 100 ms, Boltzmann fits indicated that the percentage of noninactivating current after the 100-ms conditioning pulse was greatly increased in ATX (P < 0.001).

These data demonstrate that ATX had an effect over and above that of the mutation that destabilizes fast inactivation. Not only does it slow the time course and extent of the residual inactivation in CW channels, as predicted from an effect on DIVS4 movement in addition to alterations that may arise from the CW mutation itself, but it also appears to modulate other aspects of channel gating. Among the possibilities are that ATX directly alters the voltage dependence of activation, the single-channel open probability, and/or the single-channel conductance of mutant channels, any or all of which could contribute to the increased currents observed.

With this information in hand, we examined the influence of an open-channel blocker on the amplitudes and kinetics of WT and CW currents, in the presence and absence of ATX. In these experiments, the intracellular solution included a free peptide derived from the cytoplasmic tail of the endogenous blocking protein $Na_V\beta4$ ("the β4 peptide"). This peptide reliably blocks and unblocks neuronal Na channels, inducing resurgent current (Grieco et al., 2005; Aman et al., 2009; Bant and Raman, 2010). We first tested whether intracellular application of the β4 peptide affected activation and inactivation properties of Na currents in WT and CW channels ±ATX (Fig. 2, A–F). In a subset of conditions, the β4 peptide produced small changes in the $V_{1/2}$ and k of activation and inactivation curves (Tables 1 and 2). A larger effect of the β4 peptide, however, was to reduce the amount of steady-state current through CW channels in ATX, as estimated by Boltzmann fits of inactivation (Table 2). This result is consistent with its known action as an open-channel blocker, quantified below. Therefore, although it is impossible to rule out pore-independent interactions of the peptide with these channels, these results suggest that the β4 peptide had only minor effects on gating unrelated to its role as an open-channel blocker.

In WT channels in ATX-free solutions, the β4 peptide did not change either the decay rate of currents or the current at 100 ms (Fig. 3, A, C, and E). Even at +30 mV, where the driving force on Na is low and pore block is the most stable (Aman and Raman, 2010), the 25% decay time was unchanged (control, 0.17 ± 0.01 ms; β4, 0.16 ± 0.02 ms; n = 6, 5; P = 0.6; unpaired), suggesting that the on-rate of block is not significantly faster than the onset of fast inactivation in these channels. In contrast, when macroscopic inactivation was slowed by ATX, the β4 peptide accelerated the 25% decay time at +30 mV, from 0.77 ± 0.10 ms to 0.30 ± 0.03 ms (P < 0.005). Nevertheless, the β4 peptide did not bring the extent of decay to ATX-free WT values, as the current after 100 ms

TABLE 2

Parameters of inactivation

Condition	−β4 Peptide			+β4 Peptide			P-value (−β4 vs. +β4)		
	$V_{1/2}$	k	SS (%)	$V_{1/2}$	k	SS (%)	$V_{1/2}$	k	SS (%)
	mV	*mV*		*mV*	*mV*				
WT − ATX (n = 6, 5)	−63.2 ± 0.8	5.6 ± 0.1	4.4 ± 0.3	−63.0 ± 1.1	5.7 ± 0.3	2.9 ± 0.7	0.9	0.8	0.1
WT + ATX (n = 6, 5)	−65.8 ± 1.8	8.4 ± 0.3	3.9 ± 0.4	−65.5 ± 2.2	8.0 ± 0.3	3.5 ± 0.7	0.9	0.4	0.6
CW − ATX (n = 5, 6)	−51.6 ± 2.1	14.5 ± 0.8	27.1 ± 2.4	−53.2 ± 1.5	13.6 ± 0.5	31.4 ± 1.3	0.4	0.2	0.2
CW + ATX (n = 5, 6)	−48.9 ± 1.2	7.3 ± 0.7	60.6 ± 1.2	−43.5 ± 1.6	10.5 ± 1.1	46.7 ± 1.7	<0.05	<0.05	<0.001

at +30 mV remained relatively high in ATX (control, 1.8 ± 0.5%; β4, 1.3 ± 0.4%; P = 0.45).

In CW channels, the peptide accelerated the decay of currents at all positive voltages (Fig. 3, B and D), consistent with the prediction that the β4 peptide has ample opportunity to bind to open channels when fast inactivation is diminished (Wang et al., 2006). However, the β4 peptide did not greatly affect the current at 100 ms (Fig. 3 F), suggesting that the near-equilibrium occupancy of blocked states was not significantly higher than that of residual inactivated states of the CW mutant. Even at +30 mV, where block is expected to be most stable, the β4 peptide did not significantly decrease availability at 100 ms (control, 14.0 ± 1.9%; β4, 11.3 ± 1.2%; P = 0.25). In ATX, the β4 peptide induced a fast component of current decay. Interestingly, it also decreased the current at 100 ms in a voltage-dependent manner, with the efficacy of peptide block being highest at positive potentials and becoming progressively less at negative potentials (Fig. 3, B and F). This near-linearity is consistent with observations that the ability of Na ions to displace the endogenous blocking protein varies directly with driving force (Aman and Raman, 2010).

The ability of the β4 peptide to accelerate current decay in both WT and CW channels in ATX confirms that the blocker gains access to the channel, even when DIVS4 deployment is restricted. However, β4 peptide–induced decay of currents was both more rapid and more complete without ATX. For example, even at +30 mV, the time to 25% decay in CW channels with the β4 peptide was 0.87 ± 0.11 ms in control and 1.84 ± 0.36 ms in ATX (n = 6; P = 0.02), and the current at 100 ms was 11.3 ± 1.2% in control and 20.6 ± 1.7% in ATX (P < 0.005). Because fast inactivation in CW channels is unlikely to interfere with blocker binding, one interpretation of these results is that although accessibility of the blocker is high in ATX, stability of block is reduced.

To further assess both accessibility and stability of block, we measured the effects of ATX exposure and the CW mutation on β4 peptide–induced resurgent currents. The potential was first stepped to 0 mV to provide a reference measurement of the transient current in each cell (Fig. 4 A, left). After recovery, the voltage was stepped beyond the Na^+ reversal potential to +60 mV for 10 ms to maximize open-channel block if the β4 peptide was present (Aman and Raman, 2010). The membrane was then repolarized to a series of negative potentials (Fig. 4, A, right, and B) either to evoke tail currents (without β4 peptide) or to displace the blocker and produce resurgent current (with β4 peptide). Without peptide, WT $Na_V1.4$ inactivated completely during the 10-ms conditioning pulse. Because no tail current could be clearly resolved, we quantified the data by averaging the current over the first 100 µs of repolarization. This current at −30 mV was 0.91 ± 0.40% of the transient current at 0 mV (Fig. 4, A, black, and B, top traces). With the β4 peptide, only tiny resurgent currents were elicited upon repolarization (Fig. 4, A, black, and B, bottom traces); the resurgent current at −30 mV was 5.2 ± 0.8% of the transient current measured at 0 mV, further demonstrating that the β4 peptide competes poorly with fast inactivation in $Na_V1.4$. In addition, the resurgent current rose in 1.16 ± 0.15 ms and had a decay τ of 4.55 ± 0.16 ms (Fig. 4, D–F; n = 5). These time courses are two- to threefold faster than β4

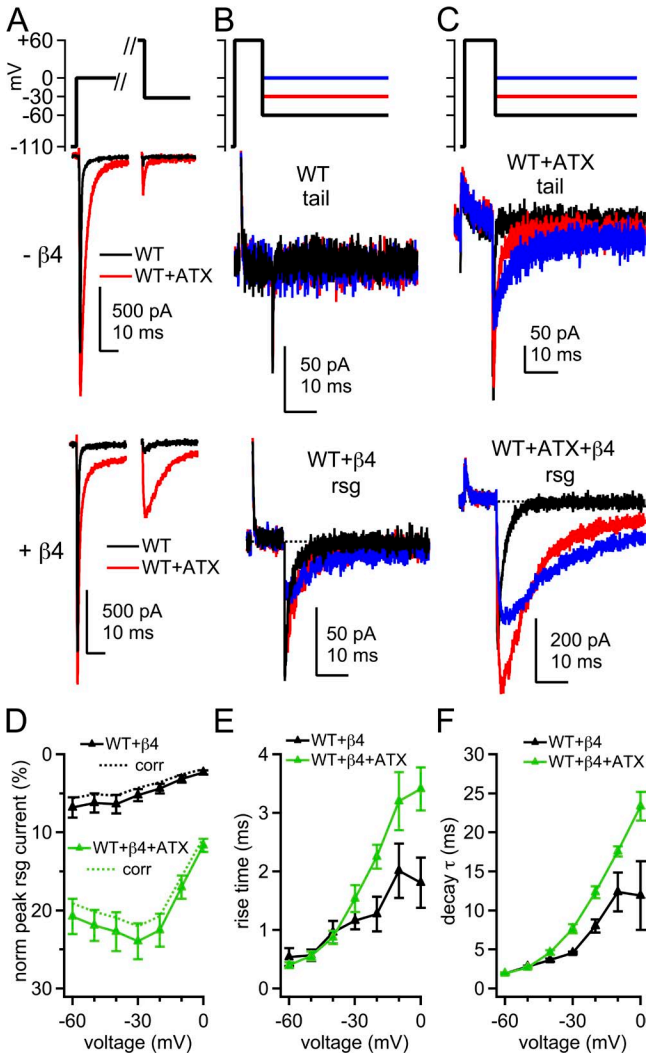

Figure 4. Tail currents and β4 peptide–induced resurgent Na currents in WT channels. (A) Voltage protocol and representative transient and tail and/or resurgent currents in WT channels without and with β4 peptide. Black, control; red, ATX. (B) Tail and resurgent currents in control solutions, as in A, expanded. (C) Tail and resurgent currents in ATX, as in A, expanded. (D) Mean peak resurgent current amplitude versus voltage in WT (black) and ATX-modified WT (green) channels. Currents normalized to peak transient current at 0 mV in each cell. Dashed lines, corrected for incomplete activation of transient current at 0 mV. (E) Mean time to peak resurgent current versus voltage. (F) Mean decay time constant (τ) of resurgent current, fit with a single exponential. Within-cell comparisons ±ATX; −β4, n = 6; +β4, n = 5.

peptide unblock in hippocampal neurons (Lewis and Raman, 2011). The rapid rise may result from a lower affinity blockade of expressed $Na_V1.4$ than of native neuronal channels, and the brief decay is likely to reflect the onset of inactivation after unbinding of the blocker (Raman and Bean, 2001; Lewis and Raman, 2011), which is particularly rapid in expressed $Na_V1.4$ channels.

Without the β4 peptide, ATX induced small tail currents in WT $Na_V1.4$, confirming that some channels were prevented from inactivating by the end of the 10-ms conditioning pulse (Fig. 4, A, red, and C, top traces). Upon repolarization from +60 to −30 mV, the tail currents rose nearly instantaneously to 19.2 ± 1.9% of the transient current at 0 mV, corresponding to a conductance of 11.8 ± 1.5% of G_{max}, and indicating that roughly 88% of channels inactivated during the conditioning pulse. The tail currents decayed with a τ of 1.38 ± 0.08 ms (n = 6). With the β4 peptide, ATX produced more than a fourfold increase in the resurgent current amplitude: the resurgent current at −30 mV was 23.9 ± 2.3% of the transient current at 0 mV (Fig. 4, A, red, C, bottom traces, and D). ATX also slightly slowed the rise and significantly prolonged the decay of the resurgent current at −30 mV (rise = 1.53 ± 0.23 ms; P = 0.17; decay τ = 7.65 ± 0.58 ms; P = 0.013; Fig. 4, E and F). Notably, this effect was voltage dependent; at the most negative voltages, at which currents deactivate rather than inactivate after unblocking, the rise and decay times were indistinguishable from ATX-free solutions (at −70 mV, rise: control = 0.49 ± 0.17 ms and ATX = 0.38 ± 0.06 ms; P = 0.34; decay τ: control = 1.46 ± 0.14 ms and ATX = 1.50 ± 0.05; P = 0.83). To test whether ATX directly affected deactivation, we applied 1-ms pulses to 0 mV to allow channels to open but not inactivate substantially, and then repolarized to −70 mV. In WT channels without the β4 peptide, tail currents decayed with a τ of 0.15 ± 0.01 ms; in ATX the decay τ was only slightly prolonged to 0.19 ± 0.02 ms (n = 5; P = 0.045; paired). The minor effect on deactivation is consistent with previous reports with other site-3 toxins (Hanck and Sheets, 1995). Thus, it is unlikely that the increased resurgent current at intermediate voltages was a result of a large ATX-dependent change in the transition rates from open to closed states in WT channels.

In contrast, in CW channels, currents evoked upon repolarization were much larger than in WT channels, and the effects of ATX were enhanced. Without β4 peptide, approximately half the current inactivated in 10 ms, with 52.3 ± 1.5% of the current remaining after a step to +30 mV. After steps to +60 mV, tail currents evoked upon repolarization were extremely large (Fig. 5, A, and B, top); the peak tail current at −30 mV was 164 ± 8% of the transient current at 0 mV. This tail conductance was equivalent to 78.4 ± 6.5% of G_{max}, indicating even fewer channels inactivated during 10 ms at +60 mV than at +30 mV.

Relative to ATX-free solutions, ATX nearly doubled the depolarization-activated current and further reduced the extent of inactivation, so that 87.6 ± 1.7% of the current remained after 10 ms at +30 mV. With 10-ms steps to +60 mV, currents did not inactivate at all, as reflected by the tail currents: the peak tail current amplitude at −30 mV corresponded to 100 ± 2% of G_{max}. The currents elicited by repolarization peaked nearly

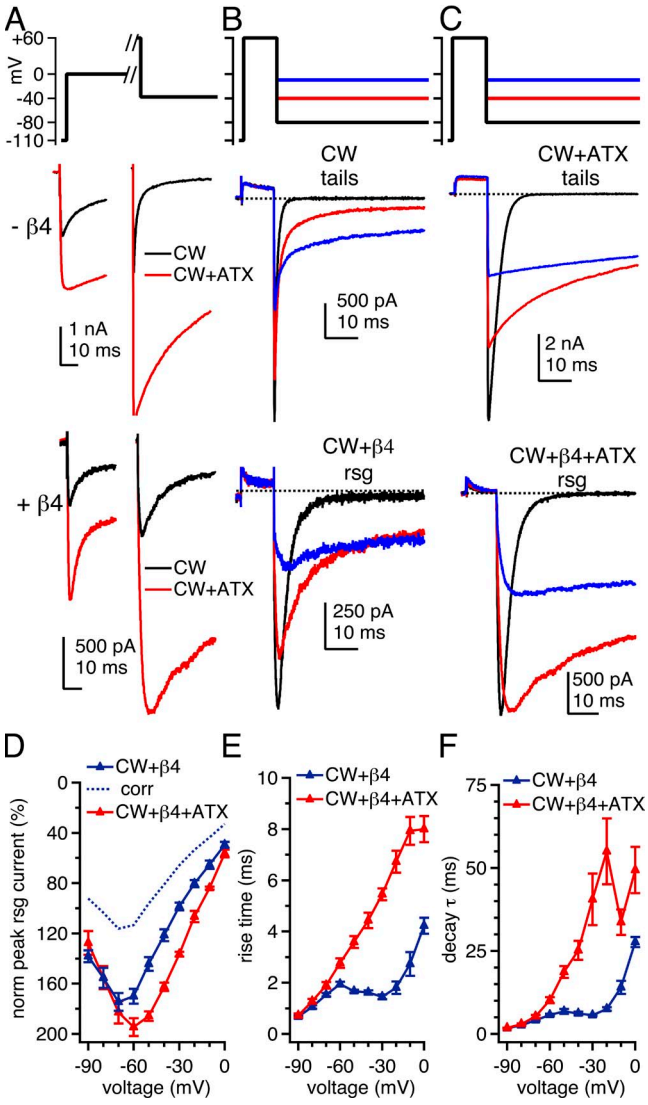

Figure 5. Tail currents and β4 peptide–induced resurgent Na currents in CW channels. (A) Voltage protocol and representative transient and tail and/or resurgent currents in CW channels, with and without β4 peptide. (B) Tail and resurgent currents in control solutions, as in A, expanded. (C) Tail and resurgent currents in ATX, as in A, expanded. (D) Mean peak resurgent current versus voltage in CW (blue) and ATX-modified CW channels (red), normalized to peak transient current at 0 mV. Dashed blue line, control data corrected for incomplete activation of the transient current at 0 mV. (E) Mean time to peak resurgent current versus voltage. (F) Mean decay time constant (τ) of resurgent current, fit with a single exponential. Within-cell comparisons ±ATX; −β4, n = 5; +β4, n = 6.

instantaneously and their amplitudes depended linearly on voltage, suggesting that they were true tail currents and not resurgent currents. Unlike in WT channels, ATX greatly slowed the macroscopic deactivation of tail currents in CW channels, even at the most negative potentials. Because this decay was bi-exponential in ATX, we quantified it as the time to 63% decay. At −30 mV, the 63% decay time for control channels was 1.6 ± 0.3 ms ($n = 5$). Remarkably, the currents in three of five ATX-modified cells failed to decay by this amount even in 100 ms, and the other two cells required 60.4 and 94.4 ms to decay by 63%. This slowing of tail current remained significant even at more negative voltages, although it occurred to a lesser degree (at −70 mV: without ATX, 0.74 ± 0.15 ms; ATX, 3.69 ± 0.79 ms; P = 0.014). These data suggest that ATX increases channel open time or burst duration but only in CW channels and not in WT channels.

The β4 peptide led CW currents to decay more quickly with depolarization and to generate resurgent-like currents with repolarization. β4-induced resurgent currents in CW channels were extremely large (Fig. 5 A, bottom, and B, bottom), and they were further increased by the addition of ATX (Fig. 5 C). Normalizing the currents at 0 mV illustrates the abnormally large resurgent-to-transient current ratio that exceeds 100% and its substantial increase by ATX; this effect is even larger when corrected for the difference in conductance at 0 mV in control and ATX-containing solutions (Fig. 5 D). As in WT channels, ATX lengthened the rise and decay times of resurgent current at voltages that favor inactivation after unblock (at −30 mV, rise time: control = 1.45 ± 0.10 ms and ATX = 5.46 ± 0.20 ms; P < 0.001; decay τ: control = 5.64 ± 0.22 ms and ATX = 40.5 ± 7.2 ms; P < 0.001; $n = 6$; paired; Fig. 5, E and F). Consistent with the ATX-induced prolongation of deactivation in CW channels, the decay τ of resurgent current in ATX was longer even at voltages that favor deactivation after unblock (at −70 mV, rise time: without ATX = 1.53 ± 0.07 ms and ATX = 1.90 ± 0.12 ms; P = 0.013; decay τ: control = 4.15 ± 0.20 and ATX = 5.29 ± 0.40; P = 0.008).

To verify that the large, resurgent-like currents evoked upon repolarization in CW channels were indeed a result of relief from open-channel block by the β4 peptide, we also measured resurgent currents using a reverse Na gradient (E_{Na} = −45 mV; Aman and Raman, 2010). Under these conditions, the reduced driving force on inwardly permeating Na ions should decrease the extent of "knock-off" of pore blockers (Armstrong, 1971; Tang et al., 1996) and thereby reduce resurgent conductance. In reverse gradients, with a conditioning pulse to +60 mV, outward currents were large and decayed rapidly as channels were blocked by the peptide (Fig. 6, A and B). Unlike in control gradients, however, little resurgent-like current was evoked upon repolarization to 0 mV, where currents remained outward.

To compare the resurgent currents in the two conditions, we measured the conductance upon repolarization at the peak of the current ("peak") and after 100 ms of repolarization ("SS") and normalized these values to the tail conductance immediately after repolarization ("tail"). Larger normalized peak conductances reflect more newly opened channels, whereas larger normalized SS conductances reflect a higher near-equilibrium occupancy of nonconducting states. In control gradients without ATX, the peak conductance was 2.6 ± 0.6–fold greater than the tail conductance, and the SS conductance was 1.1 ± 0.3 times the tail conductance ($n = 6$; Fig. 6, A and C). In ATX, the peak conductance was 2.6 ± 0.3–fold greater than the tail conductance, and the SS conductance was 1.9 ± 0.2 times the tail conductance ($n = 6$; Fig. 6, B and D). Thus, with or without ATX, many channels unblock upon repolarization from +60 to 0 mV. They then enter inactivated or closed states, but to a lesser extent in ATX than in control solutions.

In reverse gradients, the relative peak conductances were much smaller. Without ATX, the relative peak conductance was only 1.3 ± 0.03, and the relative SS

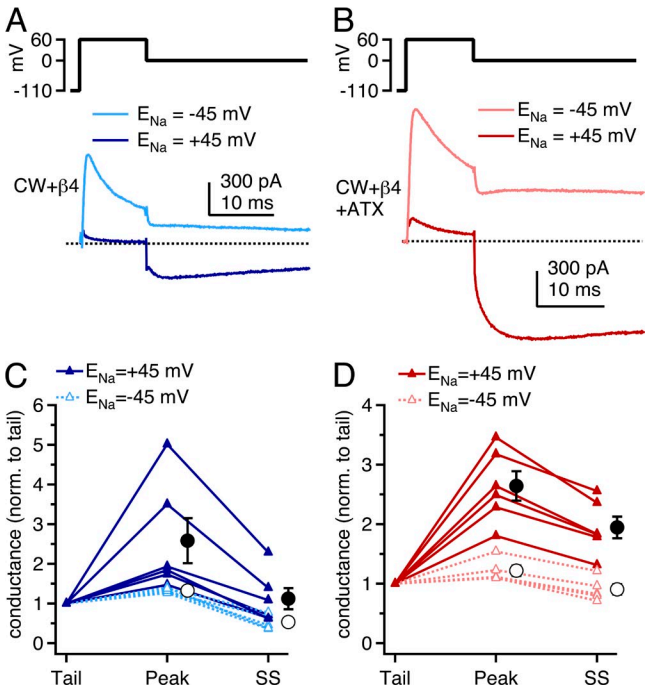

Figure 6. β4 peptide–induced resurgent Na currents in CW channels in control and reverse gradients. (A) Voltage protocol and mean repolarization-evoked currents in CW channels with the β4 peptide with E_{Na} = +45 mV (dark blue; $n = 6$) and with E_{Na} = −45 mV (light blue; $n = 6$) gradients. (B) As in A, with ATX (dark red, E_{Na} = +45 mV; light red, E_{Na} = −45 mV). (C) Tail, peak, and steady-state (SS) conductances after stepping from +60 to 0 mV, normalized for each cell to the tail conductance. Closed circles, mean for E_{Na} = +45 mV; open circles, mean for E_{Na} = −45 mV. Control, $n = 6$; reverse, $n = 5$. (D) As in C, in the presence of ATX.

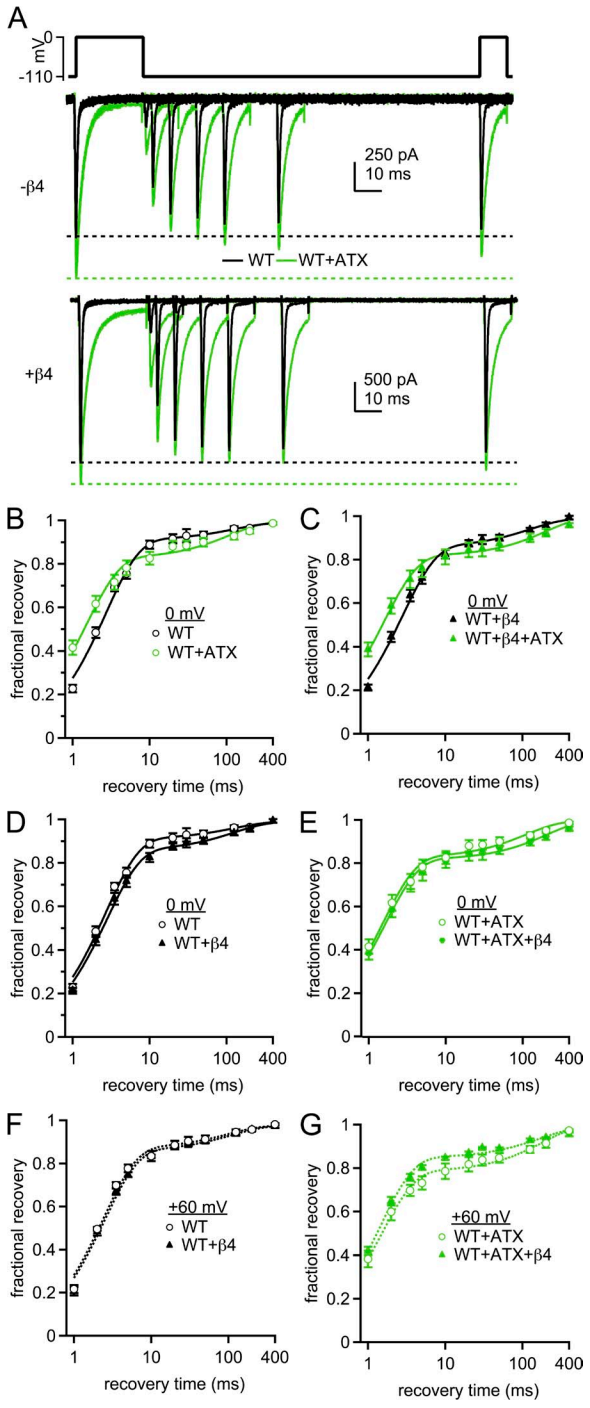

Figure 7. Time course of recovery from inactivation and from block by the β4 peptide in WT channels. (A) Voltage protocol (top) and representative cells showing recovery from inactivation and block after conditioning for 25 ms at 0 mV in the absence (middle) and presence (bottom) of the β4 peptide. Black, control; green, with 500 nM ATX. (B) Fractional recovery at 0 mV as a function of time at −110 mV. Currents were normalized to the response to the conditioning pulse for each trace, and fractional recovery was calculated as described in Materials and methods. Black, WT; green, WT plus ATX; solid lines, double-exponential fits to the mean data. (C) As in B, with β4 peptide in the intracellular solution. (D) Comparison of recovery in solutions ±β4 peptide. (E) Comparison of recovery in ATX ±β4 peptide. Within-cell comparisons ±ATX; WT, $n = 8$; WT plus β4, $n = 7$. (F and G) As in D and E, but with conditioning for 10 ms at +60 mV; without peptide, $n = 4$; with peptide, $n = 5$.

conductance fell to 0.5 ± 0.08. Similarly, in ATX, the normalized peak conductance was 1.2 ± 0.09, and the normalized SS conductance was 0.9 ± 0.09. The smaller relative conductances are indicative of a lower proportion of nonconducting channels returning to open states upon repolarization, consistent with the idea that the resurgent-like current in CW channels with the β4 peptide results from a pore blockade that is susceptible to displacement by inwardly permeating Na ions (Aman and Raman, 2010).

When comparing the resurgent currents in normal gradients in the different conditions of Fig. 5, it is evident that the β4 peptide provides an inefficient block of WT $Na_V1.4$ channels, which can be made more effective by slowing macroscopic fast inactivation by either ATX or the CW mutation. The two manipulations are, however, not identical. In WT channels, the kinetics of resurgent current are similar with and without ATX at strongly negative voltages where channels deactivate (e.g., Fig. 4, E and F), suggesting that the ATX-mediated increase in resurgent current may not depend heavily on an increase in channel open time as defined by deactivation. Instead, the increase likely results from the ATX-dependent delay of fast inactivation, which is expected to have two effects. Upon depolarization, the slowed onset of inactivation should produce a greater probability of channel block, and upon repolarization to moderate voltages, it should permit multiple reopenings before channels enter fast-inactivated states (Grieco and Raman, 2004). In contrast, even in ATX-free conditions, the CW mutation produces relatively larger β4-induced resurgent currents, suggesting that fast inactivation in ATX-modified WT channels, although slowed in its onset, measurably attenuates resurgent currents. The currents flowing upon repolarization are likely also augmented in CW channels by tail current through channels that remain open at the end of the depolarizing step, as open-channel block upon depolarization remains incomplete in CW channels, even with binding of the peptide relatively unimpeded by fast inactivation.

The observation that ATX further augments resurgent current in CW channels suggests that it has additional actions beyond the destabilization of inactivation. At least four more mechanisms by which ATX may increase resurgent current can be proposed. First, ATX may accelerate open-channel block at positive potentials. This scenario seems unlikely, however, given that the onset of β4-induced current decay upon depolarization is slower with ATX than without it (see Fig. 3, B and D), suggesting that the blocker binds but apparently not

more easily. Second, in the CW mutant, ATX may extend the mean channel open time and/or burst duration not only by delaying residual fast inactivation (as in WT channels) but also by slowing deactivation (unlike in WT channels). Third, the increase may relate to different conductance states favored by ATX, considered further in the Discussion.

A fourth possibility is that the restriction of DIVS4 deployment by ATX may change the affinity of the channel for the β4 peptide. Whether an increase or a decrease in affinity is more likely to enlarge resurgent currents cannot be predicted with certainty, however. On the one hand, an increase in affinity could lead to a greater probability of channels being blocked at the end of the conditioning pulse, so that more channels contribute to resurgent current. On the other hand, a decrease in affinity could also enlarge resurgent currents. Although fewer channels would be blocked, weaker binding would accelerate blocker expulsion upon repolarization. If channels unblock more synchronously than without ATX, the peak resurgent current may be augmented. Generally, the rise time of resurgent current is an indicator of affinity (Raman and Bean, 2001; Lewis and Raman, 2011); however, that measurement is rendered ambiguous here because inactivation rates are not constant, and instead, the ATX-dependent prolongation of channel open times lengthens the apparent rise time of the current.

We therefore investigated the influence of ATX on the affinity of the β4 peptide by examining recovery from inactivated and/or blocked states. For these experiments, a strongly negative recovery potential of −110 mV was used to ensure that, after unblock, deactivation rather than inactivation was favored during the recovery interval. Cells were stepped to 0 mV for 25 ms to open channels and allow them to make transitions into inactivated and/or blocked states. After a 1- to 400-ms recovery interval at −110 mV, availability was tested by a step to 0 mV. Because the extent of current decay varied widely across the different conditions (WT vs. CW, ±ATX, and ±β4 peptide), availability was calculated as the fraction of current that had recovered relative to the fraction of current that had become nonconducting during the conditioning pulse (see Materials and methods).

For peptide-free WT cells, recovery was rapid: after a 10-ms recovery interval, 86.1 ± 1.8% of the inactivated current was available (n = 8; Fig. 7, A–E). Recovery followed a double exponential, with a τ_{fast} of 2.7 ± 0.1 ms, accounting for 89 ± 2% recovery, and a τ_{slow} of 149 ± 21 ms (Table 3). These measurements are consistent with previous data demonstrating that most $Na_V1.4$ channels undergo fast inactivation on this time frame, with a small additional component of slow inactivation (Featherstone et al., 1996; Webb et al., 2009).

Recovery of the same currents in ATX was also fast: 80.9 ± 3.2% of the nonconducting current recovered after 10 ms. In fact, the initial phase of recovery was faster in ATX than in control, although more current recovered with a slow time constant (τ_{fast} = 1.6 ± 0.1 ms; 80 ± 2%; τ_{slow} = 111 ± 25 ms; P < 0.001, P < 0.01, and P = 0.4 vs. no ATX; n = 8). These data are consistent with previous reports that site-3 toxins accelerate recovery from fast inactivation and that more channels enter slow-inactivated states when fast inactivation is disrupted (Chahine et al., 1996; Benzinger et al., 1999).

The recovery profiles both in control and in ATX remained largely unchanged by the β4 peptide (Fig. 7, D and E, and Table 3), which could result if recovery from block occurs with a rate identical to recovery from fast

TABLE 3

Parameters of recovery from inactivation and/or block

Condition	−ATX			+ATX			P-value (−ATX vs. +ATX)		
	τ_{fast}	% τ_{fast}	τ_{slow}	τ_{fast}	% τ_{fast}	τ_{slow}	τ_{fast}	% τ_{fast}	τ_{slow}
	ms		*ms*	*ms*		*ms*			
0 mV									
WT (n = 8)	2.7 ± 0.1	89 ± 2	149 ± 21	1.6 ± 0.1	80 ± 2	111 ± 25	<0.001	<0.01	0.4
WT + β4 (n = 7)	2.8 ± 0.1	86 ± 2	118 ± 19	1.6 ± 0.1	81 ± 3	171 ± 36	<0.001	0.1	0.3
P (−β4 vs. +β4)	0.6	0.4	0.3	0.9	0.7	0.2			
CW (n = 7)	5.1 ± 0.5	47 ± 3	189 ± 15	n/a	n/a	278 ± 38	n/a	n/a	0.1
CW + β4 (n = 7)	3.1 ± 0.1	65 ± 4	205 ± 21	1.4 ± 0.1	77 ± 3	272 ± 54	<0.001	<0.001	0.3
P (−β4 vs. +β4)	<0.005	<0.005	0.6	n/a	n/a	0.9			
+60 mV									
WT (n = 4)	2.4 ± 0.1	89 ± 3	94 ± 16	1.5 ± 0.1	79 ± 3	174 ± 21	<0.05	<0.01	<0.01
WT + β4 (n = 5)	2.5 ± 0.1	88 ± 1	133 ± 36	1.4 ± 0.1	85 ± 3	185 ± 34	<0.005	0.4	<0.05
P (−β4 vs. +β4)	0.5	0.7	0.4	0.7	0.1	0.8			
CW (n = 6)	6.4 ± 1.7	25 ± 6	205 ± 18	n/a	n/a	261 ± 58	n/a	n/a	0.4
CW + β4 (n = 7)	0.8 ± 0.1	66 ± 4	184 ± 20	0.6 ± 0.1	81 ± 3	148 ± 53	<0.005	<0.05	0.5
P (−β4 vs. +β4)	<0.005	<0.001	0.5	n/a	n/a	0.2			

inactivation and/or if block itself is ineffective under these conditions. The latter possibility seems likely, as even conditioning at +60 mV for 10 ms, which should maximize blocker binding, yields small resurgent currents. After a longer step to a less depolarized potential (25 ms at 0 mV), even fewer channels are likely to be blocked at the end of the conditioning pulse. In fact, in ATX, the current remaining at the end of the 25-ms step is actually greater with than without the β4 peptide, as though the peptide antagonizes inactivation without itself binding (ATX alone: 3.4 ± 0.5%; ATX plus β4 peptide: 5.5 ± 0.6%; P = 0.01; see also Bant and Raman, 2010). Thus, it seems likely that, with a conditioning pulse to 0 mV, WT channels ±ATX recover from the same states that are favored in the absence of β4.

Therefore, to increase the probability that channels entered and remained in blocked states during the conditioning pulse, we repeated these experiments with a 10-ms step to +60 mV (Raman and Bean, 2001; Aman and Raman, 2007). Because this voltage is close to reversal (approximately +45 mV), a direct repolarization to 0 mV, which we called a "0-ms recovery step," was used to quantify the proportion of current remaining at the end of the conditioning pulse (see Materials and methods). Even with this protocol, the recovery profile for WT channels, with and without the β4 peptide, and with and without ATX, resembled the corresponding measures after a 25-ms pulse to 0 mV (Fig. 7, F and G, and Table 3). The data provide further evidence that the β4 peptide is a poor pore blocker of WT $Na_V1.4$ channels in ATX-free solutions, even with voltage steps that maximize open-channel block. In ATX, however, open-channel block does occur, evident by the resurgent currents evoked by repolarization (see Fig. 4). Therefore, the time course of recovery from conditioning at +60 mV is likely to give an accurate measure of the recovery from β4 peptide blockade and turns out to be indistinguishable from the (accelerated) recovery from fast inactivation in ATX.

We next repeated the recovery experiments in CW channels. With peptide-free solutions, currents decayed to 40.9 ± 2.3% during a conditioning pulse to 0 mV (n = 7; Fig. 8, A and B). Although less current inactivated than in WT, the inactivated fraction recovered slowly, by only 41.1 ± 3.3% after 10 ms at −110 mV. Fits of the recovery curves revealed a τ_{fast} of 5.1 ± 0.5 ms (47 ± 3%) and a τ_{slow} of 189 ± 15 ms (P < 0.001, P < 0.001, and P = 0.17 vs. WT; Fig. 8 C and Table 3). The decreased fraction of rapid recovery, which suggests that slow inactivation accounts for a greater proportion of current decay, is consistent with previous experimental disruptions of fast inactivation, including studies of this mutant channel (Featherstone et al., 1996; Wang et al., 2003).

When the same cells were exposed to ATX, the decay during the conditioning step was further reduced, so that 92.1 ± 0.7% of the current remained (Fig. 8, A and B). Strikingly, however, test currents were smaller than the current at the end of the conditioning step, leading to a negative estimate of recovery of nonconducting channels over a period of ∼100 ms. Thus, few, if any, channels recover during the interval at −110 mV. In addition, transitions into nonconducting states apparently proceed as the test current activates, leading to fewer channels

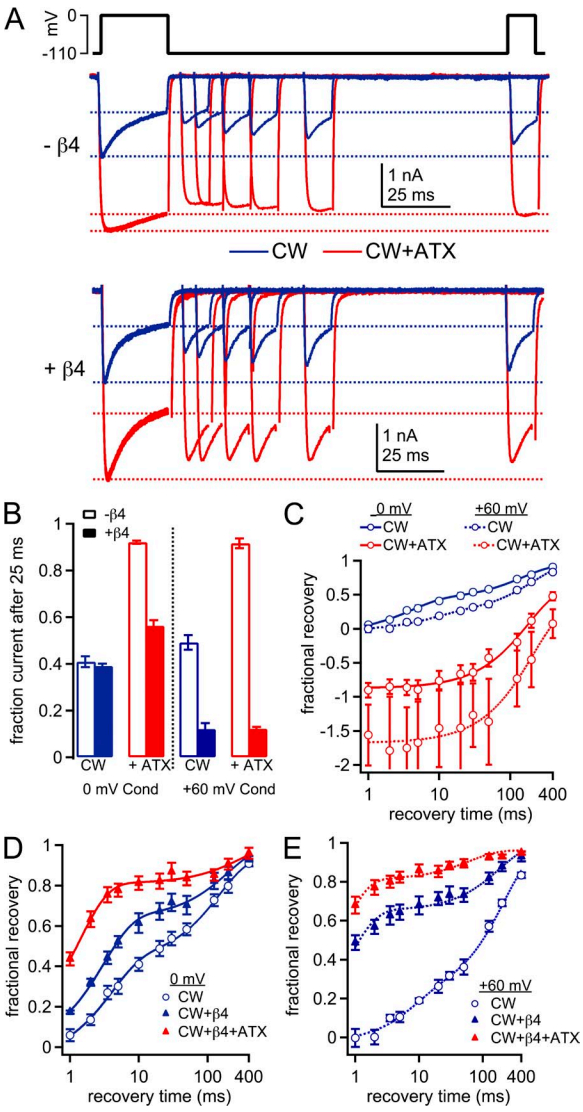

Figure 8. Time course of recovery from inactivation and from block by the β4 peptide in CW channels. (A) Voltage protocol (top) and representative cells showing recovery from inactivation and blocked states in the absence (middle) and presence (bottom) of the β4 peptide. Blue, control; red, with 500 nM ATX. (B) Fraction of current remaining at the end of the 25-ms conditioning step, normalized to peak current. (C) Fractional recovery at 0 mV as a function of time at −110 mV. Normalization and fractional recovery calculated as in Fig. 7. Blue, CW; red, CW plus ATX. The mean recovery data were fit as in Fig. 7; solid lines, conditioning at 0 mV; dotted lines, conditioning at +60 mV. (D) As in C, peptide-free, ATX-free (open blue symbols), plus β4 peptide, ATX-free (closed blue symbols); and plus β4 and ATX (solid red symbols); n = 7. (E) As in D, but after conditioning at +60 mV; without peptide, n = 6; with peptide, n = 7.

open at the peak of the test current than at the end of the conditioning pulse (see Aldrich et al., 1979). The total recovery phase was best fit with a single exponential (τ = 278 ± 38 ms; Fig. 8 C). Collectively, these data support the idea that fast inactivation is still present, although unstable, in CW channels; ATX nearly abolishes fast inactivation, leaving only slow inactivation, even though only a small proportion of channels apparently undergoes this transition.

In CW channels with the β4 peptide in ATX-free solutions, currents decayed to 60.1 ± 1.2% during the conditioning pulse (Fig. 8, A and B); this value was not significantly different from the peptide-free control (n = 7; P = 0.58). The profile of recovery was different, however, especially at short intervals. At 10 ms, recovery increased from 41.1 ± 3.3% to 62.1 ± 4.2% (P < 0.005; Fig. 8, A and D). Fitting the full curve indicated that τ_{fast} was significantly briefer and accounted for a greater fraction of recovery than without the peptide (3.1 ± 0.1 ms; 65 ± 4%; Table 3). The difference from the peptide-free condition is consistent with the presence of a distinct nonconducting state, most likely the β4 peptide–bound state. Comparing the τ_{fast} values (5.1 and 3.1 ms, without and with β4) indicates that recovery from block is at least as rapid as that from fast inactivation, even with fast inactivation destabilized by the CW mutation. Additionally, the smaller fraction of slowly recovering current seen with the β4 peptide suggests that, like the endogenous blocker in Purkinje cells, the β4 peptide may protect channels from slow inactivation (Aman and Raman, 2007).

In the presence of ATX, the β4 peptide also accelerated recovery from nonconducting states in CW channels (Fig. 8, A and B). During the conditioning pulse, the currents decayed to 58.0 ± 2.7% of the peak. The onset of decay was more rapid and its extent was greater than without β4. Recovery at brief intervals was increased relative to ATX-free solutions, with 78.4 ± 4.0% recovery after 10 ms; fits to the full recovery period gave a τ_{fast} of 1.4 ± 0.1 ms (77 ± 3%) and a τ_{slow} of 272 ± 54 ms (P < 0.001, P < 0.001, and P = 0.31 vs. no ATX; n = 7; Fig. 8 E and Table 3).

The recovery experiments in CW channels were repeated with a 25-ms conditioning pulse to +60 mV, again to maximize the number of channels remaining blocked throughout the conditioning pulse. With neither the β4 peptide nor ATX, availability at the end of the conditioning step, calculated from the 0-ms recovery step, was slightly greater than the availability of 41% after an equal period at 0 mV (49.2 ± 3.1%; P = 0.053). Also relative to 0 mV, a significantly lower percentage of current recovered with a fast time constant (τ_{fast} = 6.4 ± 1.7 ms, 25 ± 6%; τ_{slow} = 205 ± 18 ms; n = 6; P = 0.45, P < 0.01, and P = 0.49 vs. 0 mV; Fig. 8 C and Table 3). These data again demonstrate that fast inactivation is more effectively abolished when current through CW channels is outward (Wang et al., 2004).

With the addition of ATX, availability at the end of the +60-mV conditioning step increased to 91.6 ± 2.1% (n = 6; P = 0.81 vs. 0 mV; Fig. 8 C and Table 3). The time course of recovery was well fit with a single exponential, with τ = 261 ± 58 ms (P = 0.80 vs. 0 mV). Thus, ATX again abolished the small amount of fast inactivation that remained at +60 mV, leaving only slow inactivation.

Parallel experiments were done with the β4 peptide. Relative to peptide-free conditions, the β4 peptide reduced the availability at the end of the +60-mV conditioning step (12.0 ± 2.6%; n = 7; P < 0.001) and accelerated recovery in control solutions (Fig. 8 D). Fits to the full dataset gave a τ_{fast} of 0.77 ± 0.02 ms (68 ± 4%) and a τ_{slow} of 183 ± 26 ms. Notably, τ_{fast} was faster than at 0 mV (P < 0.001), with no difference in the fractional fast recovery (P = 0.89). The addition of ATX did not affect availability during the 0-ms recovery step (15.3 ± 3.1%; P = 0.67), but it did further accelerate recovery: fitting gave a τ_{fast} of 0.48 ± 0.04 ms (83 ± 3%) and a τ_{slow} of 155 ± 62 ms (P < 0.01, P < 0.05, and P = 0.5 vs. no ATX; n = 7). Although the values of the ultra-brief fast time constants are unlikely to be precisely resolved, the fact that the amount of recovery at 10 ms is raised by the β4 peptide and increased further by ATX is unambiguous (recovery at 10 ms: control vs. ATX, 67.9 ± 4.6% vs. 86.0 ± 3.1%; P < 0.001). Notably, at both conditioning voltages tested with the β4 peptide, not only did ATX shorten τ_{fast}, but it also increased the fraction of current that recovered with the more rapid time constant. Thus, although the blocker binds to ATX-modified channels at depolarized potentials, it unbinds more readily upon repolarization, accelerating recovery. The simplest explanation for this result is that ATX reduces the affinity of the channel for the β4 peptide.

DISCUSSION

These results provide evidence that open-channel block associated with resurgent Na current is influenced not only by fast inactivation but also by the DIV voltage sensor. Destabilizing binding of the fast-inactivation gate facilitates open-channel block by the β4 peptide, consistent with the previous inference that entry into fast-inactivated states and pore block by the endogenous blocking protein are mutually exclusive (Raman and Bean, 1997, 2001; Khaliq et al., 2003; Grieco and Raman, 2004). The present data further demonstrate that, even with fast inactivation disrupted, the efficacy of channel block and unblock is modulated by ATX, which influences the movement of DIVS4. When DIVS4 deployment is restricted by ATX, the β4 peptide can enter and obstruct the permeation pathway, but its binding is less stable than when DIVS4 can shift to the fully activated position. The data are consistent with the proposal that Na channels can exhibit two open states, dependent on DIVS4 position, which differ in their affinities for the blocking protein.

Inactivation in the CW mutant $Na_V1.4$ channel

To distinguish the effects of DIVS4 movement from association of the fast-inactivation gate with the channel, we made use of inactivation-deficient channels. As described previously (Wang et al., 2003), macroscopic inactivation is greatly reduced in channels with tryptophan and cysteine substitutions in DIS6. The properties of residual inactivation in these mutant channels can vary both with isoform and with Na gradient (Wang et al., 2004, 2006). Here, we find that with two such substitutions in the $Na_V1.4$ channel, and with E_{Na} at +45 mV, the macroscopic inward currents decay slowly but substantially. Some fraction of the decay likely reflects slow inactivation, as a major component of recovery proceeds with a time constant >100 ms. Fast inactivation is not altogether lost, however, as half the current recovers rapidly. Additionally, unlike in the closely related WCW $Na_V1.4$ mutant ($rNa_V1.4$-L435W/L437C/A438W; Goldschen-Ohm et al., 2013), steady-state inactivation is evident even at potentials too hyperpolarized to activate the current, suggesting that the remaining fast inactivation can proceed from closed states (Bean, 1981; Armstrong, 2006).

ATX nearly abolished the residual fast inactivation in CW channels, leaving only a small component of slow inactivation. This behavior presents a notable contrast with ATX-modified WT channels, which indeed undergo fast inactivation, albeit more slowly than in ATX-free solutions. Another major difference between WT and CW channels is that ATX produces a greater increase in peak current amplitudes and larger hyperpolarization of activation in CW channels. Both changes may stem in part from further relief of fast inactivation and/or increases in channel open time, as suggested by the ATX-mediated prolongation of deactivation in CW channels only; the macroscopic conductance change may also result from alterations in single-channel conductance (Goldschen-Ohm et al., 2013). ATX may exert these effects through multiple structural mechanisms, not limited to its interaction with DIV.

Open-channel block, the CW mutation, and ATX

Despite the potentially diverse actions of ATX, the description of WT and CW currents with and without the toxin provides a framework for examining how the open-channel blocker responsible for resurgent Na current interacts with different channel states. WT $Na_V1.4$ is a particularly poor receptor for the β4 peptide, such that little resurgent current flows upon repolarization, in part because the onset of fast inactivation is rapid in $Na_V1.4$ compared with neuronal isoforms (O'Leary, 1998). The rapid inactivation limits the number of channels that are blocked during the conditioning step and also truncates the resurgent current upon repolarization, as unblocked channels quickly becoming nonconducting (Raman and Bean, 2001; Grieco and Raman, 2004; Lewis and Raman, 2011); even endogenous blockers do not effectively block this subunit (Cummins et al., 2005; Jarecki et al., 2010). Additionally, the β4 peptide has an apparently lower affinity for expressed subunits and channels in cells lacking native resurgent current than for channels in neurons with endogenous open-channel blocking proteins (Grieco et al., 2005; Aman et al., 2009; Bant and Raman, 2010; Lewis and Raman, 2011), thus further reducing the occupancy of blocked states.

Nevertheless, manipulations that disrupt the onset or stability of fast inactivation—either the CW mutation, ATX application, or both—are permissive for open-channel block and subsequent resurgent current. The fact that ATX-modified channels generate large resurgent currents suggests that full deployment of DIVS4 is not necessary for the onset of block. In contrast, binding of the fast-inactivation gate is facilitated by, or may even require, DIVS4 deployment (Chahine et al., 1994; Sheets et al., 1999; Campos et al., 2008). The divergence may provide insight into the mechanism by which the native open-channel blocker "beats" the fast-inactivation gate to a mutually exclusive binding site in some channels but not others: if activation of the DI, DII, and DIII voltage sensors opens the channel before DIVS4 activates, it is possible that the open-channel blocking protein transiently has preferential access to a pore-occluding site. The fact that CW channels produce large resurgent currents even without ATX, however, suggests that the blocker may be able to bind even after DIVS4 has moved, as long as the channel is not occupied by the fast-inactivation gate.

Regardless of the channel conformation at the onset of open-channel block, channels eventually enter a state in which open-channel block is more stable, as recovery of β4 peptide–bound channels is accelerated by ATX. This state is likely to be distinct from the fast-inactivated state because ATX-modified CW channels without the β4 peptide show no fast recovery phase, suggesting a complete suppression of fast inactivation. Thus, blocked channels appear able to exist in two states: a higher affinity open-blocked state with DIVS4 likely deployed and a lower affinity open-blocked state with DIVS4 likely resting or only partially deployed. The latter state would usually exist only transiently but appears favored by ATX application.

Multiple open states and resurgent current

The basis for the difference in affinity is not directly addressed by these experiments, but at least two possibilities can be considered. One possibility is that the conformation of DIVS4 directly influences the accessibility or other attributes of the blocker binding site. An additional nonexclusive possibility relates to the effects of DIVS4 on permeation. Na channels display subconductances that may reflect the existence of two open

states, particularly when inactivation is limited (Nagy, 1987; Patlak, 1988). These events also occur, though rarely, in unaltered channels (Patlak, 1988; Goldschen-Ohm et al., 2013). Evidence for Na channels with multiple open states that depend on the extent of DIVS4 deployment has been shown with fluorescence data, modeling, toxin studies, and single-channel studies (Cha et al., 1999; Armstrong, 2006; Campos et al., 2008; Goldschen-Ohm et al., 2013). Of most relevance to the present study, in the WCW inactivation-deficient mutant channel, the time course of entry from a high conductance open state, O (∼17 pS), into a lower conductance state, S2 (∼13 pS), overlaps with that of DIVS4 movement as tracked by fluorescence, suggesting that the two conductance levels correspond to different states of DIVS4 deployment (Goldschen-Ohm et al., 2013). Because fast inactivation usually proceeds rapidly after full deployment of DIVS4, however, the S2 state is obscured in Na channels with intact fast inactivation. Collectively, these findings may partially account for the large increase in current amplitudes observed when ATX is applied to CW channels: without ATX, channels that are open at the peak of the current may largely be in low conductance states, whereas with ATX, the stabilization of DIVS4 in a partially deployed state may favor high conductance states.

If this is the case, it could explain the reduced affinity of the open-channel blocker in ATX. Unbinding of the blocker, and the resultant resurgent current, depends on Na influx that displaces the blocking protein from a binding site in the permeation pathway (Afshari et al., 2004; Aman and Raman, 2010). If the channel itself is in a high conductance state, the increased flow of ions would more readily expel the blocker, creating an apparently lower affinity state.

An interesting question, therefore, becomes whether or not DIVS4 must return to its resting position for the blocker to unbind. The present data provide indirect evidence that a return is not required. The extreme increase in current amplitudes when ATX is added to CW channels is consistent with the idea that a putative low conductance state is unmasked by the CW mutation (from conduction with DIVS4 deployed), but that high conductance states are rendered long-lived upon ATX application (from conduction with DIVS4 incompletely deployed). The facts that the β4 peptide can block both ATX-bound and ATX-free CW channels and that ATX increases the transient current conductance in the presence and absence of the peptide suggest that the blocker may bind to channels in either the low or high conductance state. Upon repolarization, the unusually large resurgent currents in CW channels are made still larger by ATX, probably in part to the increase in channel open time or burst duration at voltages that normally favor inactivation (Chahine et al., 1996; Benzinger et al., 1999). If ATX-free CW channels had to return to a high conductance state before (or as) the peptide unbound, they would be more likely to produce resurgent currents more closely matching the amplitudes of those in ATX-bound channels, at least at hyperpolarized potentials at which the rise and decay times are equivalent. Even at the most negative voltages (those that favor deactivation), however, ATX disproportionately increases the resurgent current relative to the transient current rather than vice versa (Fig. 5 D), suggesting that the resurgent currents in CW channels were likely carried by channels in the same low conductance states that carried the transient currents, and therefore that DIVS4 did not return to a resting position as the blocker was expelled.

It is worth noting, however, that in Purkinje cells, which endogenously express resurgent current, single channels that opened upon repolarization had the same conductance (∼20 pS) as those that opened upon depolarization (Raman and Bean, 1997), suggesting that the open state just preceding channel block was the same as that passed through upon channel unblock. On the present line of reasoning, these would both be high conductance states, but many variables may have contributed to this observation, including the presence of fast inactivation, the specific α subunits, and the tethering of the blocking protein or other Purkinje-specific factors. Interestingly, ATX reduces the macroscopic conductance of transient Na currents in frog nodes and hippocampal neurons, even while prolonging their decay times (Ulbricht and Schmidtmayer, 1981; Bant et al., 2013), suggesting that cell or subunit variability in subconductance dependence of DIVS4 position is likely to exist. Nevertheless, ATX applied to Purkinje cells enlarges native resurgent currents and accelerates their rise times in a manner consistent with a reduction in blocker affinity (Bant et al., 2013).

The present experiments thus make predictions about the action of the native blocking protein in neurons that endogenously produce resurgent current. The generation of resurgent current requires that the blocking protein binds in the permeation pathway before the fast-inactivation gate reaches its own binding site; here, we find evidence that the β4 peptide can bind before DIVS4 fully deploys, whereas the fast-inactivation gate must wait. The α subunits or Na channel complexes in which DIVS4 movement is delayed with respect to that of other domains therefore may be more likely to generate robust resurgent currents with an open-channel blocker present. The eventual deployment of DIVS4, however, further stabilizes open-channel block, thus providing further protection against fast inactivation when its onset is most likely.

We thank Dr. Steve Cannon for the kind gift of $hNa_V1.4$ and members of the Raman Laboratory, especially Dr. Jason S. Bant, for helpful discussion.

This work is supported by National Institutes of Health grants F31-NS076238 (to A.H. Lewis) and R01-NS39395 (to I.M. Raman).

Kenton J. Swartz served as editor.

Submitted: 1 March 2013
Accepted: 18 July 2013

REFERENCES

Afshari, F.S., K. Ptak, Z.M. Khaliq, T.M. Grieco, N.T. Slater, D.R. McCrimmon, and I.M. Raman. 2004. Resurgent Na currents in four classes of neurons of the cerebellum. *J. Neurophysiol.* 92: 2831–2843. http://dx.doi.org/10.1152/jn.00261.2004

Aldrich, R.W., Jr., P.A. Getting, and S.H. Thompson. 1979. Inactivation of delayed outward current in molluscan neurone somata. *J. Physiol.* 291:507–530.

Aman, T.K., and I.M. Raman. 2007. Subunit dependence of Na channel slow inactivation and open channel block in cerebellar neurons. *Biophys. J.* 92:1938–1951. http://dx.doi.org/10.1529/biophysj.106.093500

Aman, T.K., and I.M. Raman. 2010. Inwardly permeating Na ions generate the voltage dependence of resurgent Na current in cerebellar Purkinje neurons. *J. Neurosci.* 30:5629–5634. http://dx.doi.org/10.1523/JNEUROSCI.0376-10.2010

Aman, T.K., T.M. Grieco-Calub, C. Chen, R. Rusconi, E.A. Slat, L.L. Isom, and I.M. Raman. 2009. Regulation of persistent Na current by interactions between β subunits of voltage-gated Na channels. *J. Neurosci.* 29:2027–2042. http://dx.doi.org/10.1523/JNEUROSCI.4531-08.2009

Armstrong, C.M. 1971. Interaction of tetraethylammonium ion derivatives with the potassium channels of giant axons. *J. Gen. Physiol.* 58:413–437. http://dx.doi.org/10.1085/jgp.58.4.413

Armstrong, C.M. 2006. Na channel inactivation from open and closed states. *Proc. Natl. Acad. Sci. USA.* 103:17991–17996. http://dx.doi.org/10.1073/pnas.0607603103

Bant, J.S., and I.M. Raman. 2010. Control of transient, resurgent, and persistent current by open-channel block by Na channel beta4 in cultured cerebellar granule neurons. *Proc. Natl. Acad. Sci. USA.* 107:12357–12362. http://dx.doi.org/10.1073/pnas.1005633107

Bant, J.S., T.K. Aman, and I.M. Raman. 2013. Antagonism of lidocaine inhibition by open-channel blockers that generate resurgent Na current. *J. Neurosci.* 33:4976–4987. http://dx.doi.org/10.1523/JNEUROSCI.3026-12.2013

Bean, B.P. 1981. Sodium channel inactivation in the crayfish giant axon. Must channels open before inactivating? *Biophys. J.* 35:595–614. http://dx.doi.org/10.1016/S0006-3495(81)84815-1

Benzinger, G.R., G.S. Tonkovich, and D.A. Hanck. 1999. Augmentation of recovery from inactivation by site-3 Na channel toxins. A single-channel and whole-cell study of persistent currents. *J. Gen. Physiol.* 113:333–346. http://dx.doi.org/10.1085/jgp.113.2.333

Campos, F.V., B. Chanda, P.S. Beirão, and F. Bezanilla. 2008. α-Scorpion toxin impairs a conformational change that leads to fast inactivation of muscle sodium channels. *J. Gen. Physiol.* 132:251–263. http://dx.doi.org/10.1085/jgp.200809995

Cha, A., P.C. Ruben, A.L. George Jr., E. Fujimoto, and F. Bezanilla. 1999. Voltage sensors in domains III and IV, but not I and II, are immobilized by Na^+ channel fast inactivation. *Neuron.* 22:73–87. http://dx.doi.org/10.1016/S0896-6273(00)80680-7

Chahine, M., A.L. George Jr., M. Zhou, S. Ji, W. Sun, R.L. Barchi, and R. Horn. 1994. Sodium channel mutations in paramyotonia congenita uncouple inactivation from activation. *Neuron.* 12:281–294. http://dx.doi.org/10.1016/0896-6273(94)90271-2

Chahine, M., E. Plante, and R.G. Kallen. 1996. Sea anemone toxin (ATX II) modulation of heart and skeletal muscle sodium channel alpha-subunits expressed in tsA201 cells. *J. Membr. Biol.* 152:39–48. http://dx.doi.org/10.1007/s002329900083

Chanda, B., and F. Bezanilla. 2002. Tracking voltage-dependent conformational changes in skeletal muscle sodium channel during activation. *J. Gen. Physiol.* 120:629–645. http://dx.doi.org/10.1085/jgp.20028679

Cummins, T.R., S.D. Dib-Hajj, R.I. Herzog, and S.G. Waxman. 2005. Nav1.6 channels generate resurgent sodium currents in spinal sensory neurons. *FEBS Lett.* 579:2166–2170. http://dx.doi.org/10.1016/j.febslet.2005.03.009

Eaholtz, G., T. Scheuer, and W.A. Catterall. 1994. Restoration of inactivation and block of open sodium channels by an inactivation gate peptide. *Neuron.* 12:1041–1048. http://dx.doi.org/10.1016/0896-6273(94)90312-3

el-Sherif, N., H.A. Fozzard, and D.A. Hanck. 1992. Dose-dependent modulation of the cardiac sodium channel by sea anemone toxin ATXII. *Circ. Res.* 70:285–301. http://dx.doi.org/10.1161/01.RES.70.2.285

Featherstone, D.E., J.E. Richmond, and P.C. Ruben. 1996. Interaction between fast and slow inactivation in Skm1 sodium channels. *Biophys. J.* 71:3098–3109. http://dx.doi.org/10.1016/S0006-3495(96)79504-8

Goldschen-Ohm, M.P., D.L. Capes, K.M. Oelstrom, and B. Chanda. 2013. Multiple pore conformations driven by asynchronous movements of voltage sensors in a eukaryotic sodium channel. *Nat Commun.* 4:1350. http://dx.doi.org/10.1038/ncomms2356

Grieco, T.M., and I.M. Raman. 2004. Production of resurgent current in NaV1.6-null Purkinje neurons by slowing sodium channel inactivation with beta-pompilidotoxin. *J. Neurosci.* 24:35–42. http://dx.doi.org/10.1523/JNEUROSCI.3807-03.2004

Grieco, T.M., J.D. Malhotra, C. Chen, L.L. Isom, and I.M. Raman. 2005. Open-channel block by the cytoplasmic tail of sodium channel β4 as a mechanism for resurgent sodium current. *Neuron.* 45:233–244. http://dx.doi.org/10.1016/j.neuron.2004.12.035

Hanck, D.A., and M.F. Sheets. 1995. Modification of inactivation in cardiac sodium channels: Ionic current studies with Anthopleurin-A toxin. *J. Gen. Physiol.* 106:601–616. http://dx.doi.org/10.1085/jgp.106.4.601

Horn, R., S. Ding, and H.J. Gruber. 2000. Immobilizing the moving parts of voltage-gated ion channels. *J. Gen. Physiol.* 116:461–476. http://dx.doi.org/10.1085/jgp.116.3.461

Jarecki, B.W., A.D. Piekarz, J.O. Jackson II, and T.R. Cummins. 2010. Human voltage-gated sodium channel mutations that cause inherited neuronal and muscle channelopathies increase resurgent sodium currents. *J. Clin. Invest.* 120:369–378. http://dx.doi.org/10.1172/JCI40801

Khaliq, Z.M., N.W. Gouwens, and I.M. Raman. 2003. The contribution of resurgent sodium current to high-frequency firing in Purkinje neurons: an experimental and modeling study. *J. Neurosci.* 23:4899–4912.

Klinger, A.B., M. Eberhardt, A.S. Link, B. Namer, L.K. Kutsche, E.T. Schuy, R. Sittl, T. Hoffmann, C. Alzheimer, T. Huth, et al. 2012. Sea-anemone toxin ATX-II elicits A-fiber-dependent pain and enhances resurgent and persistent sodium currents in large sensory neurons. *Mol. Pain.* 8:69. http://dx.doi.org/10.1186/1744-8069-8-69

Lewis, A.H., and I.M. Raman. 2011. Cross-species conservation of open-channel block by Na channel β4 peptides reveals structural features required for resurgent Na current. *J. Neurosci.* 31:11527–11536. http://dx.doi.org/10.1523/JNEUROSCI.1428-11.2011

Liu, P., S. Jo, and B.P. Bean. 2012. Modulation of neuronal sodium channels by the sea anemone peptide BDS-I. *J. Neurophysiol.* 107:3155–3167. http://dx.doi.org/10.1152/jn.00785.2011

Long, S.B., E.B. Campbell, and R. Mackinnon. 2005. Voltage sensor of Kv1.2: structural basis of electromechanical coupling. *Science.* 309:903–908. http://dx.doi.org/10.1126/science.1116270

Nagy, K. 1987. Subconductance states of single sodium channels modified by chloramine-T and sea anemone toxin in neuroblastoma cells. *Eur. Biophys. J.* 15:129–132. http://dx.doi.org/10.1007/BF00263676

O'Leary, M.E. 1998. Characterization of the isoform-specific differences in the gating of neuronal and muscle sodium channels. *Can. J. Physiol. Pharmacol.* 76:1041–1050. http://dx.doi.org/10.1139/y98-137

Patlak, J.B. 1988. Sodium channel subconductance levels measured with a new variance-mean analysis. *J. Gen. Physiol.* 92:413–430. http://dx.doi.org/10.1085/jgp.92.4.413

Raman, I.M., and B.P. Bean. 1997. Resurgent sodium current and action potential formation in dissociated cerebellar Purkinje neurons. *J. Neurosci.* 17:4517–4526.

Raman, I.M., and B.P. Bean. 2001. Inactivation and recovery of sodium currents in cerebellar Purkinje neurons: evidence for two mechanisms. *Biophys. J.* 80:729–737. http://dx.doi.org/10.1016/S0006-3495(01)76052-3

Raman, I.M., L.K. Sprunger, M.H. Meisler, and B.P. Bean. 1997. Altered subthreshold sodium currents and disrupted firing patterns in Purkinje neurons of Scn8a mutant mice. *Neuron.* 19:881–891. http://dx.doi.org/10.1016/S0896-6273(00)80969-1

Rogers, J.C., Y. Qu, T.N. Tanada, T. Scheuer, and W.A. Catterall. 1996. Molecular determinants of high affinity binding of alpha-scorpion toxin and sea anemone toxin in the S3-S4 extracellular loop in domain IV of the Na^+ channel alpha subunit. *J. Biol. Chem.* 271:15950–15962. http://dx.doi.org/10.1074/jbc.271.27.15950

Sheets, M.F., J.W. Kyle, R.G. Kallen, and D.A. Hanck. 1999. The Na channel voltage sensor associated with inactivation is localized to the external charged residues of domain IV, S4. *Biophys. J.* 77:747–757. http://dx.doi.org/10.1016/S0006-3495(99)76929-8

Sittl, R., A. Lampert, T. Huth, E.T. Schuy, A.S. Link, J. Fleckenstein, C. Alzheimer, P. Grafe, and R.W. Carr. 2012. Anticancer drug oxaliplatin induces acute cooling-aggravated neuropathy via sodium channel subtype Na(V)1.6-resurgent and persistent current. *Proc. Natl. Acad. Sci. USA.* 109:6704–6709. http://dx.doi.org/10.1073/pnas.1118058109

Stühmer, W., F. Conti, H. Suzuki, X.D. Wang, M. Noda, N. Yahagi, H. Kubo, and S. Numa. 1989. Structural parts involved in activation and inactivation of the sodium channel. *Nature.* 339:597–603. http://dx.doi.org/10.1038/339597a0

Tang, L., R.G. Kallen, and R. Horn. 1996. Role of an S4–S5 linker in sodium channel inactivation probed by mutagenesis and a peptide blocker. *J. Gen. Physiol.* 108:89–104. http://dx.doi.org/10.1085/jgp.108.2.89

Theile, J.W., B.W. Jarecki, A.D. Piekarz, and T.R. Cummins. 2011. Nav1.7 mutations associated with paroxysmal extreme pain disorder, but not erythromelalgia, enhance Navbeta4 peptide-mediated resurgent sodium currents. *J. Physiol.* 589:597–608. http://dx.doi.org/10.1113/jphysiol.2010.200915

Ulbricht, W., and J. Schmidtmayer. 1981. Modification of sodium channels in myelinated nerve by Anemonia sulcata toxin II. *J. Physiol. (Paris).* 77:1103–1111.

Wang, G.K., T. Edrich, and S.Y. Wang. 2006. Time-dependent block and resurgent tail currents induced by mouse $\beta4_{154–167}$ peptide in cardiac Na^+ channels. *J. Gen. Physiol.* 127:277–289. http://dx.doi.org/10.1085/jgp.200509399

Wang, S.Y., K. Bonner, C. Russell, and G.K. Wang. 2003. Tryptophan scanning of D1S6 and D4S6 C-termini in voltage-gated sodium channels. *Biophys. J.* 85:911–920. http://dx.doi.org/10.1016/S0006-3495(03)74530-5

Wang, S.Y., E. Moczydlowski, and G. Wang. 2004. Inactivation-deficient human skeletal muscle Na+ channels (hNav1.4-L443C/A444W) in stably transfected HEK-293 cells. *Receptors Channels.* 10:131–138. http://dx.doi.org/10.1080/10606820490514914

Webb, J., F.F. Wu, and S.C. Cannon. 2009. Slow inactivation of the NaV1.4 sodium channel in mammalian cells is impeded by co-expression of the beta1 subunit. *Pflugers Arch.* 457:1253–1263. http://dx.doi.org/10.1007/s00424-008-0600-8

Yu, F.H., R.E. Westenbroek, I. Silos-Santiago, K.A. McCormick, D. Lawson, P. Ge, H. Ferriera, J. Lilly, P.S. DiStefano, W.A. Catterall, et al. 2003. Sodium channel beta4, a new disulfide-linked auxiliary subunit with similarity to beta2. *J. Neurosci.* 23:7577–7585.